Accepted Manuscript

Astragaloside exerts anti-photoaging effects in UVB-induced premature senescence of rat dermal fibroblasts through enhanced autophagy

Weijie Wen, Jianwen Chen, Liugang Ding, Xia Luo, Xueping Zheng, Qi Dai, Qianqian Gu, Cui Liu, Ming Liang, Xiaolei Guo, Peiqing Liu, Min Li

PII: S0003-9861(18)30475-2

DOI: 10.1016/j.abb.2018.09.007

Reference: YABBI 7807

To appear in: *Archives of Biochemistry and Biophysics*

Received Date: 13 June 2018

Revised Date: 31 July 2018

Accepted Date: 10 September 2018

Please cite this article as: W. Wen, J. Chen, L. Ding, X. Luo, X. Zheng, Q. Dai, Q. Gu, C. Liu, M. Liang, X. Guo, P. Liu, M. Li, Astragaloside exerts anti-photoaging effects in UVB-induced premature senescence of rat dermal fibroblasts through enhanced autophagy, *Archives of Biochemistry and Biophysics* (2018), doi: 10.1016/j.abb.2018.09.007.

Astragaloside exerts anti-photoaging effects in UVB-induced premature senescence of rat dermal fibroblasts through enhanced autophagy

Weijie Wen[1#], Jianwen Chen[1#], Liugang Ding[2#], Xia Luo[1], Xueping Zheng[1], Qi Dai[1], Qianqian Gu[1], Cui Liu[1], Ming Liang[2], Xiaolei Guo[2], Peiqing Liu[1*], Min Li[1*]

[1]School of Pharmaceutical Sciences, Guangdong Provincial Key Laboratory of New Drug Design and Evaluation, National and Local United Engineering Lab of Druggability and New Drugs Evaluation, Sun Yat-Sen University, Guangzhou, Guangdong 510006, China

[2]Research &Development Centre, Infinitus (China) Company Ltd, Guangzhou 510663, China

# These authors contributed equally

* Corresponding authors:

Min Li, School of Pharmaceutical Sciences, Sun Yat-Sen University, Guangzhou, Guangdong 510006, China, Phone:86-20-39943036, E-mail: limin65@mail.sysu.edu.cn

Peiqing Liu, School of Pharmaceutical Sciences, Sun Yat-Sen University, Guangzhou, Guangdong 510006, China; Phone: 86-20-39943030, E-mail: liupq@mail.sysu.edu.cn

The Conflict-of-Interest and Financial Disclosure Statements

There were no potential conflicts of interest and no significant financial support for this work to disclose

Highlights

1. UVB-induced collagen-I reduction, photoaging, oxidative stress and cytotoxicity could be partially rescued by astragaloside.

2. UVB-induced ERK and p38 activation, which is involved in UVB-induced collagen-I degradation, could be repressed by astragaloside.

3. UVB-suppressed autophagy could be reversed by astragaloside.

4. Astragaloside upregulates UVB-reduced collagen-I by enhancing autophagy.

Key words: astragaloside, autophagy, collagen, MAPK, photoaging

Abbreviations: AM, *Astragalus Membranaceus*; APS, astragalus polysaccharides; ASF, astragalus flavonoids; ASI, astragaloside IV; AST, astragaloside; Col1, collagen-I; CQ, chloroquine; 3-MA, 3-methyladenine; MAPK, mitogen-activated protein kinase; MMP, metalloproteinase; Rap, rapamycin; ROS, reactive oxygen species; UV, ultraviolet.

Number of text words: 6400 (including references and figure legends)

Number of references: 37

Number of tables: 1

Number of figures: 7

Abstract

Background: *Astragalus membranaceus* is a fundamental herb in Traditional Chinese Medicine and has attracted significant attention due to its anti-inflammatory, and longevity effects. However, its anti-photoaging property remains to be defined. Autophagy plays important roles in regulating cell homeostasis and aging processes. Whether regulation of autophagy could be an efficient way for anti-photoaging is still unclear.

Objective: To investigate the effects and the possible mechanism of astragaloside on anti-photoaging in UVB-induced photoaging cell model.

Methods: Primary rat dermal fibroblasts were prepared by repeated exposures to UVB irradiation. The expression levels of cytokines and signal molecules were determined by RT-PCR and western blot. SA-β-gal staining was performed to indicate senescence level. Intracellular reactive oxygen species and mitochondrial membrane potential were monitored by fluorescent probes DCFH-DA and JC-1. The cell viability was determined using Cell Counting Kit-8.

Results: Astragaloside increases the expression of collagen-I (Col1) downregulated by UVB. UVB-induced oxidative stress and photoaging could be inhibited by astragaloside. The degradation of Col1 caused by UVB irradiation through activated ERK and p38 signals could be suppressed by astragaloside. Importantly, autophagy was induced by astragaloside. Col1 could be further accumulated by chloroquine but decreased by 3-methyladenine in photoaged cell after treatment of astragaloside.

Conclusion: Autophagy play essential roles, at least partially, in modulating the formation and degradation of Col1 in photoaging cell model. Astragaloside increases the accumulation of Col1 and protects UVB-induced photoaging cells through not only ERK and p38 inhibition but also autophagy activation, indicating the potential application of astragaloside for anti-photoaging therapy.

Introduction

Skin aging is a complex biological process influenced by a combination of genetic and environmental factors. These factors lead to cumulative physiological and structural changes in the skin appearance [1]. Facial chronic senescence of the skin due to sunlight manifests itself as extrinsic skin aging (photoaging) and UV irradiation such as UVA and UVB which are the primary causes of accelerated photoaging. Both UVA and UVB have been shown to cause cell proliferation arrest, and apoptosis, although these responses can be context-dependent [2, 3]. UVB damages DNA directly to form photoproducts, mainly the cyclopyrimidine dimers (CPDs) [4], which accounts for most UVB-induced mutations [5] and subsequently photoaging whereas UVA exerts its most established effects on photoaging through oxidative damage to DNA, proteins, and lipids [3]. Since UVB is more cytotoxic and mutagenic than UVA radiation [6, 7], photoaging caused by UVB is a more common form of skin damage and even can result in skin carcinoma [8]. Due to the fact that skin health and beauty are considered as overall well-being and the perception of physical health in humans, many efficient anti-aging strategies have been developed to prevent photoaging, such as sun avoidance, free radicals neutralizers, herbs, and pharmacological agents with anti-aging properties [9, 10]. In the skin, fibroblasts constitute the main cell type of the dermis and are responsible for the production of the different extracellular matrix components, so dermal fibroblasts have been applied as a simplified model of aging to identify potential protective effect of various components of *Astragalus Membranaceus* (AM) *in vitro* [11].

UV irradiation activates mitogen-activated protein kinase signaling (MAPK), which involves the upregulation of extracellular signal-regulated kinases (ERK), c-Jun amino terminal kinase (JNK), and p38. The elevated levels of c-Jun and c-Fos in turn activate the transcription factor AP-1, which upregulates the expression of various matrix metalloproteinases (MMPs) [12]. Importantly, in the skin tissue MMP-1 and other proteases are responsible for the degradation of collagen-I (Col1) which has been used as a key feature of the pathophysiology of photoaging [13, 14].

Autophagy is a highly conserved cellular process that digests damaged organelles or misfolded macromolecules to facilitate cell survival and adaptation during starvation, genotoxic stress, and oxidative stress in normal cells [15]. Dysregulation of autophagy can therefore contribute to the development of a number of skin diseases and aging [16, 17]. In aging skin, the increased number

of autophagosomes found in fibroblasts are mainly caused by impaired autophagic flux, which leaded to alterations in the content of extracellular matrix proteins [18]. Given the varying of cell type and exposure time, both UVA and UVB have been reported to activate autophagy through reactive oxygen species (ROS) production (mainly under UVA irradiation) and DNA damages (mainly under UVB irradiation) [7, 19, 20], and activation of 5' adenosine monophosphate-activated protein kinase (AMPK), UV radiation resistance-associated gene protein (UVRAG), and p53 or downregulate autophagy through lysosome dysfunction [3, 21]. Several chemicals and genetic tools have been reported to prevent photoaging through either autophagy inhibition or autophagy activation [22, 23]. So autophagy modulators are of great interest to the treatment and prevention of UV-induced skin disorders and skin diseases.

AM is a well-known Chinese tonic herb. Its active ingredients are able to improve the memory of aged mice, enhance the activity of cerebral and recover neurochemical impairments induced by stress [24, 25]. The main bioactive components of AM primarily contain flavonoids, astragalosides, and polysaccharides [25]. Previous studies showed that astragalosides possessed an anti-aging and immunomodulatory effects, probably being related to its anti-oxidative properties [26]. Other contents of AM also contributed to their cardio-protective and anti-inflammatory effects [27]. Collagens in wounded skins of diabetic rat model could be faster synthesized by AM extracts [28]. However, little attention has been paid on their protective roles in skin photoaging.

In the present study, we compared the effects of different component standards of AM on UVB-induced photoaging cell model using rat primary dermal fibroblasts (RDFs). Among the different components, only astragaloside standards (AST) could enhance Col1 formation and reverse photoaging through the anti-oxidative stress and the suppression of ERK and p38 signals. More importantly, autophagy was found to be induced by AST for the first time in both normal culture cells and photoaged cells. AST could effectively promote the accumulation of Col1 reduced by UVB-irradiation through autophagy activation, indicating that targeting autophagy pathway by AST would be a potential therapeutic strategy for photoaging.

Materials and Methods

Materials

AST (Astragaloside standards, >98%, CAS: 17429-69-5), ASI (Astragaloside IV

standards, >98%, CAS: 84687-43-4), ASF (Astragalus flavone standards, >70%), and APS (Astragalus polysaccharides standards, >70%, CAS: 89250-26-0) were purchased from the National RM Source Center (Beijing, China). Antibiotics penicillin/streptomycin and fetal bovine serum for cell culture were obtained from Gibco (Grand Island, NY). The following antibodies were used for immunoblot and immunostaining: Col1 (Boster, Wuhan, China). MMP-1 (Proteintech, Wuhan, China), p21 (Proteintech), GAPDH (Proteintech), p62 (Proteintech), LC3B (Sigma, St. Louis, MO), Vimentin (Proteintech), p38 (Cell signaling, Danvers, MA), Phospho-p38 (Cell signaling), ERK (Cell signaling), phospho-ERK (Cell signaling), cleaved caspase 3 (Cell signaling), α-tubulin (Sigma). Secondary antibodies were from Life Technologies (Carlsbad, CA). 3-Metheyladenine (3-MA) was from Selleckchem (Houston, TX). Rapamycin was from LC Laboratories (Woburn, MA). Chloroquine diphosphate salt (CQ) was from Sangon（Shanghai, China）. All cell culture dishes, plates, and flasks were obtained from Corning (Corning, NY).

Preparation of rat primary dermal fibroblasts

RDFs were prepared from 1-3 day new-born Sprague-Dawley (SD) rat supplied by the Experimental Animal Center of Sun-Yat Sen University. The skin removed from SD rats was disinfected with ethanol, and then separated from the connective tissue. Then the skin tissue was put into 0.06% trypsin at 4°C overnight. After digested, the dermis could be easily separated from epidermis. The dermis was transferred to a new sterilized culture dish and cut into small pieces, then treated with 0.1% collagenase I (Thermofisher Scientific, Rockford, IL) at 37°C in a shaking incubator. After 30 min, the liquid was moved to a centrifuge tube with complete medium containing antibiotics. Secondly, the 0.06% trypsin was added to digest the rest dermis at 37°C for 5 min several times until the skin tissue was digested completely. Then pooled cells were centrifuged and seeded in dishes. Once established, all primary cell cultures were maintained in DMEM (Gibco) containing 10% of fetal bovine serum plus 100 U/mL of penicillin and 100 μg/mL of streptomycin and propagated at 37°C. Cells were split at a ratio of 1:3 for later passages. The cells from passages 3 to 8 were used in this study. The animal experiment in the current study was approved by the Research Ethics Committee of Sun Yat-Sen University.

Preparation of photoaging cell model

UVB-induced dermal fibroblast photoaging model was established according to the previous studies [29, 30]. In brief, the dosage of UVB was according to pilot experiments to act on cells.

UVB irradiation was delivered by a portable narrow band UVB lamb (Zhongyiboteng, Beijing, China) emitting at 308-311 nm wavelengths. The emitted radiation was checked at the same level of dishes using a UVR radiometer with a UVB/UVA sensor (Lutron, Taiwan). The irradiation was performed twice a day for 3 days. Control cells were kept in the same culture conditions without UVB exposure. At the end of 0-48 hours after the last stress, the cells were harvested for further analysis.

SA-β-Gal staining

To detect one of the biomarkers of senescence, senescence-associated β-galactosidase (SA-β-Gal) staining was performed [31]. After a series of 6 exposures to UVB at 4 mJ/cm^2, cells were cultivated for another 48 h in complete medium. The cells were fixed and incubated at 37°C with fresh SA-β-Gal stain solution (Beyotime, Shanghai, China). The number of SA-β-Gal-positive cells was determined by counting 500 cells in each well using the phase-contrast microscopy EVOS Original (AMG, Mill Creek, WA)，the proportions of cells positive for the SA-β-Gal activity are shown as percentage of the total number of cells counted in each well. The results are expressed as mean of triplicates ± SD.

Determination of mitochondrial membrane potential and intercellular ROS

Intracellular reactive oxygen species (ROS) were determined with 2'7'-dichlorodihydro-fluorescein diacetate (DCFH-DA) (Beyotime, China). RDFs were seeded into 96-well plates. After preloading 10 μmol/L of DCFH-DA for 30 min at 37°C, RDFs were exposed to UVB irradiation at a single dose of 10 mJ/cm^2. The signal of 2′, 7′-dichlorofluorescein (DCF, the oxidation product of DCFH-DA) was then immediately observed using the ArrayScan VII (Thermofisher, Waltham, MA) at excitation wavelength of 488 nm and emission wavelength of 525 nm. By the Build-in image analysis software, the average fluorescence intensity from randomly selected fields (60 for each group) was measured.

To monitor the mitochondrial membrane potential, a fluorescent probe JC-1 (Beyotime) was used. JC-1 can selectively enter into mitochondria and reversibly shift fluorescence color from red to green in a potential-dependent manner, which means mitochondrial membrane potential decrease. After a single dose of UVB irradiation at 10 mJ/cm^2, RDFs were incubated for another 24 hours and then treated with JC-1 for 20 min at 37°C. Subsequently, the cells were washed and respectively showed red fluorescence (Ex=485nm, Em=525nm) and green fluorescence

(Ex=525nm, Em=590nm). The digital images were photographed by ArrayScan VII and the average fluorescence intensity from randomly selected fields (60 cells per group) was measured by build-in image analysis software.

Cell viability assay

The effect of UVB on cell viability was determined using Cell Counting Kit-8 (CCK-8) (Biotool, Houston, TX) according to manufacturer's instructions. Briefly, 4×10^4 cells per well were seeded in a 96-well plate. After overnight incubation, the cells were treated with 100 mg/ml of AST for 24 h before exposed to a dose of 10 mJ/cm^2 of UVB and then cultured in DMEM for another 24 h. 10 μl of CCK-8 reagent was added to each well for 2 h. The absorbance was finally measured at 450 nm using Flex Station 3 (Molecular Device, Sunnyvale, CA). The cell viability of UVB-treated fibroblasts was described as a percentage compared to the non-treated cells, and the control cells were considered to be 100% viable.

Immunoblot and immunostaining analysis

Cells were lysed in RIPA lysis buffer (Beyotime) supplemented with protease inhibitor (Thermo). The protein concentration was determined using the BCA protein assay reagent. After denaturation, lysates with equally 20 μg to 30 μg of protein were separated by 8%–12% SDS-PAGE and transferred onto Immobilon-P Transfer Membrane (Millipore). Membranes were blocked with Tris-buffered saline with 0.1% Tween 20 (TBST) containing 5% skimmed milk (Fudebio, Najing, China) and then incubated overnight at 4°C with different primary antibodies. Detection was achieved using peroxidase-conjugated secondary antibodies and by ECL detection system-ImageQuant Las 4000 (GE, Uppsala, Sweden).

RDFs plated on coverslips were fixed with 4% paraformaldehyde for 15 min at room temperature. Permeabilization was performed with 0.1% Triton-X-100 followed by blocking with 10% goat serum solution at room temperature for 1 h. The cells were further incubated with primary antibodies of vimentin overnight at 4ºC, and then incubated with Alexa Fluor 488-labeled secondary antibodies for 1 h at room temperature. Nuclei were stained with 5 μg/ml of 4', 6-diamidino-2-phenylindole (DAPI). After washed with PBS, the coverslips were inspected with EVOS FL Auto Imaging System.

RNA extraction and real time PCR

RDFs were seeded into 6-well culture plates and treated with a series of UVB irradiation

mentioned above. At 48 h after the last stress, total cellular RNA was extracted using the RNAiso Plus (Takara, Dalian, China) and quantitated by Nanodrop 2000 (Thermo). Afterwards, the obtained RNA was converted to cDNA using Revert Aid First Strand cDNA Synthesis Kit (Thermo) by PCR thermal cycler (Eppendorf, Hamberg, Germany). The real time PCR assay was performed on iCycler iQ system (Bio-Rad, Hercules, CA) using SYBR-Green Quantitative PCR kit (Toyobo, Osaka, Japan). Sequences of the primers used in this study were listed in table 1.

Statistics

Data are presented as means ± SD of at least three independent experiments. Differences were evaluated by one-way analysis of variance post hoc Dun net's, using GraphPad Prism. A p-value of less than 0.05 was considered statistically significant.

Results

1. Establishment of a photoaging model in rat dermal fibroblasts

To establish the photoaging cell model, RDFs were isolated from skin tissue of new-born laboratory SD rat. Most of the primary cells are first identified as vimentin positive with the spindle shape and clear contour (Fig. S1A). In order to test the appropriate influence of UVB that caused RDF senescence, the SA-β-Gal staining was applied to identify the senescent cells. The percentage of positive cells in the non-UV irradiation was low but significantly high at a series of 4 mJ/cm^2 of UVB-exposure (Fig. 1A). We then compared senescence related proteins such as p21 and p53, which were hallmarks of senescent cells, and found p21 was apparently enhanced especially at the intensity of 3-5 mJ/cm^2 of repeated UVB exposures and p53 expression was also up-regulated in a dose-dependent manner. (Fig. 1B-C). Consistent to the protein expression, p21 was also confirmed by RT-PCR (Fig. 1D). To assess the regulatory effect of UVB on the production of other senescence-associated proteins in RDFs, the transcriptional changes of p16, IL-6, IL-1β and TNFα were investigated by RT-PCR. As expected, UVB irradiation increased mRNA level of those pro-inflammatory cytokines, cyclin-dependent kinase inhibitor significantly (Fig. 1D). Those findings indicated UVB irradiation could enhance senescence-related proteins and UVB-induced photoaging model using RDFs was established successfully

2. AST represses UVB-induced collagen-I reduction and photoaging

The Col1 is the dominant type of collagens found in skin. As a key marker of photoaging, the

formation and degradation of Col1 was sensitive to UVB-irradiation. As shown in figure 2A, the Col1 level of RDFs decreased gradually in a dose-dependent way under UV-irradiation. Then we compared the effect of four active ingredients of AM at the same concentration of 100 μg/ml. For photoaged RDFs, AST is the only one that could elevate the protein level of Col1 significantly (Fig. 2B). Different from the changes of Col1, both Col3 and MMP3 protein level were just slightly affected by 100 μg/ml of ASI, APS, ASF, and AST, respectively (data not shown). The remarkable role of AST in the regain or recovery of Col1 during photoaging was further confirmed by different doses of AST (Fig. 2C). However, the dose-response effect of AST on the expression level of Col1 was not observed in non-irradiated cells (data not shown). We further investigated the anti-photoaging effect of AST. Determined by the classical biomarker of cellular senescence, SA-β-Gal activity, AST could reduce the number of UVB-irradiated aged cells (Fig. 2D). Thus, AST rather than other components of AM could repress UVB-induced Col1 reduction and photoaging.

3. Protective effects of AST on oxidative stress and cytotoxicity

Since increased intracellular level of ROS is one of the main causes for cellular senescence, ROS generation in response to UVB irradiation was then evaluated using the probe of DCFDA. After the application of AST, the ROS level was markedly attenuated (Fig. 3A), indicating AST could function as an anti-oxidant. Next, the mitochondria health was detected using JC-1 staining. As shown in figure 3B, mitochondrial depolarization was indicated by a decrease in the red/green fluorescence intensity ratio after UVB-irradiation, and such depolarization could be reversed by the use of AST. Since AST shows stronger protective capability of anti-oxidative stress and mitochondria health, we want to know whether AST could in turn increase the cell viability of photoaged RDFs. As shown in figure 3C, 100 μg/ml of AST neither increased nor suppressed the cell viability significantly, however, under the stress of UVB irradiation, the application of AST could remarkably reverse the cell viability decline, which indicted the cyto-protective effect of AST against UVB irradiation. We further analyzed the protein expression level of caspase 3, an indicator of apoptosis which could be cleaved in apoptotic cells and p53, a protein that regulates the cell proliferation. In figure 3D, cleaved caspase 3 and p53 were enhanced after UVB-irradiation compared to control group. However, both proteins were reduced significantly after adding AST, suggesting AST may inhibit apoptosis and promote cell growth to enhance cell

viability. Taken together, AST could prevent photoaged RDFs from oxidative stress with mitochondria dysfunction and increase cell viability through its anti-apoptosis properties.

4. ERK and p38 signals are involved in collagen-I degradation

The effects of AST on the mRNA expression of MMPs and ICAM1 were determined using RT-PCR. Under the stress of repeated UVB irradiation to RDFs, the mRNA expression level of those pro-inflammatory cytokines IL-1β and IL-6, and cyclin-dependent kinase inhibitor p21 showed markedly increase and could be reversed after the administration of AST (Fig. 4A), but AST did not reduce TNFα transcription. Exposure of RDFs to UVB also significantly increased the mRNA expression of MMP1, 3, 9, 13 and ICAM1, and treatment of AST at 100 μg/ml could significantly reduce the transcription of MMP1 and MMP13, which both function as collagenase in rat, and MMP9 comparable to those UVB-irradiated cells without AST treatment (Fig. 4B). But ICAM1 and MMP3 did not alter when AST was applied which is consistent with the protein expression of MMP3 (data not shown). UV-irradiation could activate MAPK by increased intracellular ROS, and the digestion of collagens due to the upregulation of MMPs, subsequently leading to photoaging. As shown in figure 4C, ERK and p38 signals of MAPK subfamily were phosphorylated by UVB as expected while the application of AST dramatically attenuated such activation of ERK, p38 and Col1 degradation clearly. Considering that JNK is one of the MAPK subfamily like p38 and ERK, we also detected the activation of JNK, but we did not observe the phenomenon of JNK activation as the same as p38 in a series of doses of UVB irradiation (Fig. S1B, Fig. S1C). These findings indicated that AST could modulate Col1 through the inhibition of ERK and p38, both are well-known classic signals involved in the degradation of Col1 led by UV irradiation.

5. UVB-suppressed autophagy could be reversed by AST

Intriguingly, when RDFs were with UVB, the protein level of lipidated-LC3 (LC3-II), a widely used marker for autophagy, decreased dramatically at the doses higher than 2 mJ/cm^2 (Fig. S2A), suggesting autophagy might be suppressed by UVB irradiation. Among the four ingredients of AM, AST shows the strongest capability to rescue UVB-reduced LC3-II level (Fig. 5A). The ubiquitin-associated protein p62 that binds to LC3 can be degraded by functional autophagy. So p62 was thought as an important marker for the induction of autophagy, clearance of protein aggregates and the inhibition of autophagy [15]. In figure 5B, both the reduction of p62 and the

induction of LC3-II could be stimulated by AST in a dose-dependent manner during photoaging. Next, we measured the autophagy flux by lysosomal inhibitor CQ to elucidate the effects of AST on autophagy. As shown in figure 5C, in photoaging condition, CQ could block the degradation of basal LC3-II and further increased the level of LC3-II once AST was added. Meanwhile, the degradation of p62 was enhanced by AST, but further blocked by CQ, suggesting AST could initiate autophagy instead of blocking autophagy flux. Moreover, in non-irradiation condition, like rapamycin (Rap), AST increased the accumulation of LC3-II and the degradation of p62 in RDFs as well, indicating AST is an autophagy inducer in both normal cells and photoaged cells (Fig. 5D). The autophagy flux could be suppressed by autophagy inhibitors 3-MA and CQ at both early stage and late stage. Those data indicated UVB-irradiation inhibited autophagy initiation and AST could reverse such inhibition efficiently.

6. AST upregulated UVB-reduced collagen-I by autophagy activation

Since UVB could accelerate both Col1 reduction and autophagy inhibition (Fig. S2B), we sought to know whether autophagy was involved in Col1 formation and degradation. As shown in figure 6A, UVB-reduced autophagy could be reversed gradually by of AST in line with the regain of Col1, suggesting activating autophagy might be helpful to generate Col1. The application of 3-MA which was used to repress the early stage of autophagy induction further attenuated UVB-reduced Col1 formation compared to irradiation groups with AST (Fig. 6B). To further validate the role of autophagy in the regulation of Col1, another autophagy inhibitor CQ was used to block autophagy degradation at the late stage (Fig. 6C). In photoaged RDFs, the degradation of Col1 could be blocked by CQ alone and further accumulated when combined with AST significantly, indicating the generation and degradation of Col1 depends on the functional autophagy flux. For normal cultured cells, however, none of the autophagy inhibitors 3-MA and CQ, or autophagy inducers AST and rapamycin could significantly accumulate Col1, suggesting the protective role of autophagy in modulating Col1 formation in normal cells is different from that in photoaged cells (Fig. 6D). Altogether, these data demonstrated that inhibiting autophagy by UVB-irradiation could impair Col1 formation and exacerbate photoaging, while AST might upregulate UVB-reduced Col1 by autophagy activation.

Discussion

Naturally occurring drugs or botanical ingredients have attracted considerable attention as antiaging agents for the use of human skin care or skin diseases [9, 32]. As a popular Traditional Chines Medicine, AM has been widely used due to its anti-oxidant, anti-inflammatory, and cardio-protective properties. However, little is known about its anti-photoaging effects. In this paper we studied the protective effects of the active ingredients of AM on UVB-induced photoaging and demonstrated their probable mechanism using RDF cell model. We found AST not only reversed the decrease of cell viability and oxidative stress caused by UVB-irradiation, but also rescued the Col1 degradation through ERK and p38 but not JNK inhibition in photoaged cells. Importantly, we found UVB could suppress autophagy and reduce the formation of Col1, and such effects could be suppressed by AST due to its autophagy induction properties (Fig. 7). Our study indicated for the first time that AST could protect cells against photoaging efficiently through autophagy activation.

Skin fibroblasts are the most common cells of dermis, which play an important role in the process of photoaging [33]. For photoaging study, primary cells, rather than stable cell lines, are preferred in studies of cell senescence, apoptosis, and DNA repair, because infinite cell lines would not enter into the permanent growth arrest named replicative senescence. Therefore, UVB irradiation to primary cells could mimic the real situation of skin aging for UV exposure to the greatest extent. To avoid the interference of analysis of cell proliferative capabilities between intrinsic senescence and photoaging, the early passage primary rat dermal fibroblasts isolated from neonatal rats' dermis were suitable for the following investigation about cellar mechanism involved in UVB-induced photoaging. Although UVB irradiation is more effective than UVA in inducing skin photoaging, the specific wavelengths responsible for it are still not well known. The broad band UVB is generally thought to be the main cause of skin photoaging because of its intense influences on histological, physical, and visible skin change which are resemble to that occurring in natural skin aging [34]. However, narrow band UVB could also be used to establish both animal and cellular photoaging models even though its capability of causing photoaging is less potent [35, 36]. Therefore, it is acceptable to use the narrow band UVB for photoaging cellular model in this study. Triggered by UVB irradiation, senescent cells would be characterized by growth arrest, enlarged and fattened cell morphology, higher SA-β-Gal activity, and increased expression of cell cycle inhibitors p21, p16, and p53 [30, 33]. According to those aging markers,

AST strongly reduced the SA-β-Gal activity, p53 expression, and the apoptosis level. Although ASI was also reported to show anti-aging effects in human dermal cells [37, 38], it did not work well in this study according to the SA-β-Gal activity, which might because of the difference of cell models and irradiation stress. Even if APS and ASF showed the effect of reduction of SA-β-Gal activity as the same as AST, they performed no use to reverse the degradation of UVB-induced Col1. These results suggest AST is an efficient nature product of AM to prevent UVB-induced skin cell photoaging.

Intracellular ROS levels and oxidative stress are elevated during UV irradiation, mitochondria damage, and toxins [39]. Oxidative stress, a major risk factor underlying cellular senescence and photoaging may lead to the activation of MAPK-mediated signal pathway followed by activation of transcriptional factors NF-kB and AP-1. Then the expression of pro-inflammatory cytokines IL-1β, IL-6, and TNFα that may be involved in immune regulation and lead to photo-damage were induced [37]. Intercellular adhesion molecule-1 (ICAM-1) is another molecule involved in the inflammatory response that is overexpressed in senescent cells and aged tissues [40]. Cells undergoing senescence are also associated with overexpression of those cytokines due to an age-related redox imbalance. Antioxidant polyphenols have been shown to suppress the UV-induced pro-inflammatory cytokines of IL-1α and IL-6 in the dermis [41]. The data in this work revealed that consistent with the anti-oxidative effect, the levels of these cytokines were markedly reduced in the cells treated with AST after UVB irradiation.

Recent studies indicated that chronologically aged and UV-irradiated skin share important molecular features including altered signals that promoted MMPs expression which were mainly mediated by pro-inflammatory cytokines. Eventually, they may lead to decreased collagen synthesis, and connective tissue damage [42]. Col1 is the most abundant structure protein in the skin and connective tissue that could be degraded by MMP-1, so these properties make MMP1 and Col1 attractive targets for the pharmacological development of anti-photoaging agents [43]. It is well established that expression of MMP1 is controlled by NF-κB and AP-1 activation, which would be activated upon UV irradiation following MAPK cascades. In the present study, we showed that AST notably down-regulated UVB-induced MMP1, MMP9 and MMP13 followed by ERK and p38 activation, suggesting that ERK and p38 might be important signals for AST in regulating the formation and the degradation of Col1 during photoaging.

It has been reported that the autophagy is involved in the aging process. On the one hand, autophagy function and activity decrease in aged human dermal fibroblasts due to the impaired degradation of autophagy [18]. On the other hand, UV-induced ROS production leads to the activation of autophagy. However, our model showed long-term exposures of UVB mainly inhibited the initiation step of autophagy with a decrease of LC3-II. Microtubule-associated protein 1A/1B-light chain 3 (LC3) is a soluble protein that is ubiquitously expressed in mammalian tissues and cultured cells, which is associated with autophagy. Two forms of LC3, called LC3-I and LC3-II, were produced by post-translation in various cells. LC3-I is cytosolic whereas LC3-II is recruited to autophagosomal membranes. Thus, lysosomal turnover of the autophagosomal marker LC3-II reflects autophagic activities [44]. Those works indicated that autophagy may play complex regulatory roles in aging and photoaging stress response in different context. Among the main ingredients of AM, APS was reported to inhibit the autophagy induced by H_2O_2 in C2C12 myoblasts, and improves cardia function after IR-induced injury through reducing cardiomyocytes autophagy [45], while ASI could reverse the Ang II-induced mitochondrial dysfunction by enhancing mitochondrial autophagy [46, 47]. In addition, AST can reduce apoptosis and autophagy through decreasing the oxidative stress, ER stress and mitochondrial dysfunction in PC12 [48]. However, none of them have been studied to modulate autophagy in photoaged skin fibroblasts. Here, AST demonstrated the obvious activity to induce autophagy in both normal cells and photoaged cells with the up-regulation of autophagy flux activity. So, this work discloses a novel function of AST as an autophagy inducer in RDFs.

The most remarkable feature of photoaged skin is the loss of dermal collagen histologically [32]. When AST was applied to UVB-irradiated RDFs, similar to the pattern of autophagy regulation, the decrease of Col1 was blocked dramatically suggesting the autophagy activity might be tightly connected to the formation of Col1. Autophagy has been reported to promote intracellular degradation of Col1 to suppress kidney fibrosis in mice and affect cardia remodeling [48, 49]. However, few studies were reported on the modulation of autophagy on skin dermal fibroblasts. In photoaged RDFs, the production of Col1 required the autophagy induced by AST and could be attenuated by autophagy inhibitor 3-MA. Once the lysosome degradation was blocked by CQ, the accumulation of Col1 would be enhanced. Different from the role of autophagy in other tissues, AST-induced autophagy benefits the formation of Col1 while the degradation of Col1 also

depends on functional autophagy flux in photoaged dermal fibroblasts. Intriguingly, such Col1 accumulation could not occur in the normal cultured cells despite using autophagy inducers or inhibitors suggesting the role of autophagy in modulating the formation of Col1 might be stress-dependent.

Taken together, the present study provides the first evidence that AST protected RDFs from UVB-induced photoaging. On the one hand, UVB could induce ROS generation in the RDFs, which is critical for the photoaging progression. ROS subsequently activated MAPK subfamily of ERK and p38 but not JNK, which would inhibit col1 formation and lead to photoaging, and AST could reverse this process by alleviating ROS accumulation after UVB irradiation. On the other hand, UVB-induced photoaging repressed the autophagic activities and AST, as an autophagy inducer, initialed autophagy in both normal RDFs and photoaged RDFs, thus AST enables the autophagy flux to be functional in photoaged RDFs. So AST also performs its anti-photoaging effects and accelerates col1 formation through the regulation of autophagy (Fig. 7). Based on these findings, AST could have good potential as an anti-photoaging agent for therapy purpose. However, it should also be noted that the results of this study were based on experiments performed using *in vitro* cellular model. Accordingly, further studies using in *vivo* animal models would be considered. In addition, to separate the herbal monomers of AM would be helpful to understand their function in depth such as their roles in autophagy regulation.

Acknowledgments

This work was supported by the National Natural Science Foundation of China (31671437), the Natural Science Foundation of Guangdong Province, China (2016A030313335), the National Science and Technology Major Project of the Ministry of Science and Technology of China (2018ZX09735010), and the Guangdong Provincial Key Laboratory of Construction Foundation (2017B030314030).

References

[1] J. Uitto, Understanding premature skin aging, N Engl J Med 337(20) (1997) 1463-5.

[2] J. D'Orazio, S. Jarrett, A. Amaro-Ortiz, T. Scott, UV radiation and the skin, Int J Mol Sci 14(6) (2013) 12222-48.

[3] A. Sample, Y.Y. He, Autophagy in UV Damage Response, Photochem Photobiol 93(4) (2017) 943-955.

[4] T. Matsunaga, K. Hieda, O. Nikaido, Wavelength dependent formation of thymine dimers and (6-4) photoproducts in DNA by monochromatic ultraviolet light ranging from 150 to 365 nm, Photochem Photobiol 54(3) (1991) 403-10.

[5] S. Nakajima, L. Lan, S. Kanno, M. Takao, K. Yamamoto, A.P. Eker, A. Yasui, UV light-induced DNA damage and tolerance for the survival of nucleotide excision repair-deficient human cells, J Biol Chem 279(45) (2004) 46674-7.

[6] H. Ikehata, Mechanistic considerations on the wavelength-dependent variations of UVR genotoxicity and mutagenesis in skin: the discrimination of UVA-signature from UV-signature mutation, Photochem Photobiol Sci (2018).

[7] T. Budden, N.A. Bowden, The role of altered nucleotide excision repair and UVB-induced DNA damage in melanomagenesis, Int J Mol Sci 14(1) (2013) 1132-51.

[8] D. McDaniel, P. Farris, G. Valacchi, Atmospheric skin aging-Contributors and inhibitors, J Cosmet Dermatol 17(2) (2018) 124-137.

[9] R. Ganceviciene, A.I. Liakou, A. Theodoridis, E. Makrantonaki, C.C. Zouboulis, Skin anti-aging strategies, Dermatoendocrinol 4(3) (2012) 308-19.

[10] R.R. Korac, K.M. Khambholja, Potential of herbs in skin protection from ultraviolet radiation, Pharmacogn Rev 5(10) (2011) 164-73.

[11] T. He, T. Quan, G.J. Fisher, Ultraviolet irradiation represses TGF-beta type II receptor transcription through a 38-bp sequence in the proximal promoter in human skin fibroblasts, Exp Dermatol 23 Suppl 1 (2014) 2-6.

[12] M. Fanjul-Fernandez, A.R. Folgueras, S. Cabrera, C. Lopez-Otin, Matrix metalloproteinases: evolution, gene regulation and functional analysis in mouse models, Biochim Biophys Acta 1803(1) (2010) 3-19.

[13] T. Quan, Z. Qin, W. Xia, Y. Shao, J.J. Voorhees, G.J. Fisher, Matrix-degrading metalloproteinases in photoaging, J Investig Dermatol Symp Proc 14(1) (2009) 20-4.

[14] G.J. Fisher, Z.Q. Wang, S.C. Datta, J. Varani, S. Kang, J.J. Voorhees, Pathophysiology of premature skin aging induced by ultraviolet light, N Engl J Med 337(20) (1997) 1419-28.

[15] N. Mizushima, Autophagy: process and function, Genes Dev 21(22) (2007) 2861-73.

[16] R.J. Chen, Y.H. Lee, Y.L. Yeh, Y.J. Wang, B.J. Wang, The Roles of Autophagy and the Inflammasome during Environmental Stress-Triggered Skin Inflammation, Int J Mol Sci 17(12) (2016).

[17] C. Scherfer, V.C. Han, Y. Wang, A.E. Anderson, M.J. Galko, Autophagy drives epidermal deterioration in a Drosophila model of tissue aging, Aging (Albany NY) 5(4) (2013) 276-87.

[18] K. Tashiro, M. Shishido, K. Fujimoto, Y. Hirota, K. Yo, T. Gomi, Y. Tanaka, Age-related disruption of autophagy in dermal fibroblasts modulates extracellular matrix components, Biochem Biophys Res Commun 443(1) (2014) 167-72.

[19] S. Mouret, C. Baudouin, M. Charveron, A. Favier, J. Cadet, T. Douki, Cyclobutane pyrimidine dimers are predominant DNA lesions in whole human skin exposed to UVA radiation, Proc Natl Acad Sci U S A 103(37) (2006) 13765-70.

[20] A.P. Schuch, N.C. Moreno, N.J. Schuch, C.F.M. Menck, C.C.M. Garcia, Sunlight damage to cellular DNA: Focus on oxidatively generated lesions, Free Radic Biol Med 107 (2017) 110-124.

[21] S.D. Lamore, G.T. Wondrak, Autophagic-lysosomal dysregulation downstream of cathepsin B inactivation in human skin fibroblasts exposed to UVA, Photochem Photobiol Sci 11(1) (2012) 163-72.

[22] X. Chen, M. Li, L. Li, S. Xu, D. Huang, M. Ju, J. Huang, K. Chen, H. Gu, Trehalose, sucrose and raffinose are novel activators of autophagy in human keratinocytes through an mTOR-independent pathway, Sci Rep 6 (2016) 28423.

[23] Z. Qiu, B. Kuhn, J. Aebi, X. Lin, H. Ding, Z. Zhou, Z. Xu, D. Xu, L. Han, C. Liu, H. Qiu, Y. Zhang, W. Haap, C. Riemer, M. Stahl, N. Qin, H.C. Shen, G. Tang, Discovery of Fluoromethylketone-Based Peptidomimetics as Covalent ATG4B (Autophagin-1) Inhibitors, ACS Med Chem Lett 7(8) (2016) 802-6.

[24] K.K. Auyeung, Q.B. Han, J.K. Ko, Astragalus membranaceus: A Review of its Protection Against Inflammation and Gastrointestinal Cancers, Am J Chin Med 44(1) (2016) 1-22.

[25] J. Fu, Z. Wang, L. Huang, S. Zheng, D. Wang, S. Chen, H. Zhang, S. Yang, Review of the botanical characteristics, phytochemistry, and pharmacology of Astragalus membranaceus (Huangqi), Phytother Res 28(9) (2014) 1275-83.

[26] H. Lei, B. Wang, W.P. Li, Y. Yang, A.W. Zhou, M.Z. Chen, Anti-aging effect of astragalosides and its mechanism of action, Acta Pharmacol Sin 24(3) (2003) 230-4.

[27] X. Ma, K. Zhang, H. Li, S. Han, Z. Ma, P. Tu, Extracts from Astragalus membranaceus limit myocardial cell death and improve cardiac function in a rat model of myocardial ischemia, J Ethnopharmacol 149(3) (2013) 720-8.

[28] Y. Yang, F. Wang, D. Yin, Z. Fang, L. Huang, Astragulus polysaccharide-loaded fibrous mats promote the restoration of microcirculation in/around skin wounds to accelerate wound healing in a diabetic rat model, Colloids Surf B Biointerfaces 136 (2015) 111-8.

[29] J.P. Zeng, B. Bi, L. Chen, P. Yang, Y. Guo, Y.Q. Zhou, T.Y. Liu, Repeated exposure of mouse dermal fibroblasts at a sub-cytotoxic dose of UVB leads to premature senescence: a robust model of cellular photoaging, J Dermatol Sci 73(1) (2014) 49-56.

[30] F. Permatasari, Y.Y. Hu, J.A. Zhang, B.R. Zhou, D. Luo, Anti-photoaging potential of Botulinum Toxin Type A in UVB-induced premature senescence of human dermal fibroblasts in vitro through decreasing senescence-related proteins, J Photochem Photobiol B 133 (2014) 115-23.

[31] F. Debacq-Chainiaux, J.D. Erusalimsky, J. Campisi, O. Toussaint, Protocols to detect senescence-associated beta-galactosidase (SA-betagal) activity, a biomarker of senescent cells in culture and in vivo, Nat Protoc 4(12) (2009) 1798-806.

[32] I. Binic, V. Lazarevic, M. Ljubenovic, J. Mojsa, D. Sokolovic, Skin ageing: natural weapons and strategies, Evid Based Complement Alternat Med 2013 (2013) 827248.

[33] F. Debacq-Chainiaux, C. Borlon, T. Pascal, V. Royer, F. Eliaers, N. Ninane, G. Carrard, B. Friguet, F. de Longueville, S. Boffe, J. Remacle, O. Toussaint, Repeated exposure of human skin fibroblasts to UVB at subcytotoxic level triggers premature senescence through the TGF-beta1 signaling pathway, J Cell Sci 118(Pt 4) (2005) 743-58.

[34] D.L. Bissett, D.P. Hannon, T.V. Orr, Wavelength dependence of histological, physical, and visible changes in chronically UV-irradiated hairless mouse skin, Photochem Photobiol 50(6) (1989) 763-9.

[35] A.M. Altman, J. Bankson, N. Matthias, J.V. Vykoukal, Y.H. Song, E.U. Alt, Magnetic resonance imaging as a novel method of characterization of cutaneous photoaging in a murine model, Arch Dermatol Res 300(5) (2008) 263-7.

[36] Y.S. Tian, N.H. Kim, A.Y. Lee, Antiphotoaging effects of light-emitting diode irradiation on narrow-band ultraviolet B-exposed cultured human skin cells, Dermatol Surg 38(10) (2012)

1695-703.

[37] M.J. Hong, E.B. Ko, S.K. Park, M.S. Chang, Inhibitory effect of Astragalus membranaceus root on matrix metalloproteinase-1 collagenase expression and procollagen destruction in ultraviolet B-irradiated human dermal fibroblasts by suppressing nuclear factor kappa-B activity, J Pharm Pharmacol 65(1) (2013) 142-8.

[38] B. Yang, C. Ji, X. Chen, L. Cui, Z. Bi, Y. Wan, J. Xu, Protective effect of astragaloside IV against matrix metalloproteinase-1 expression in ultraviolet-irradiated human dermal fibroblasts, Arch Pharm Res 34(9) (2011) 1553-60.

[39] M. Cavinato, P. Jansen-Durr, Molecular mechanisms of UVB-induced senescence of dermal fibroblasts and its relevance for photoaging of the human skin, Exp Gerontol 94 (2017) 78-82.

[40] V.G. Gorgoulis, H. Pratsinis, P. Zacharatos, C. Demoliou, F. Sigala, P.J. Asimacopoulos, A.G. Papavassiliou, D. Kletsas, p53-dependent ICAM-1 overexpression in senescent human cells identified in atherosclerotic lesions, Lab Invest 85(4) (2005) 502-11.

[41] J.A. Nichols, S.K. Katiyar, Skin photoprotection by natural polyphenols: anti-inflammatory, antioxidant and DNA repair mechanisms, Arch Dermatol Res 302(2) (2010) 71-83.

[42] L. Rittie, G.J. Fisher, UV-light-induced signal cascades and skin aging, Ageing Res Rev 1(4) (2002) 705-20.

[43] G.J. Fisher, S. Kang, J. Varani, Z. Bata-Csorgo, Y. Wan, S. Datta, J.J. Voorhees, Mechanisms of photoaging and chronological skin aging, Arch Dermatol 138(11) (2002) 1462-70.

[44] I. Tanida, T. Ueno, E. Kominami, LC3 and Autophagy, Methods Mol Biol 445 (2008) 77-88.

[45] Y. Yin, L. Lu, D. Wang, Y. Shi, M. Wang, Y. Huang, D. Chen, C. Deng, J. Chen, P. Lv, Y. Wang, C. Li, L.B. Wei, Astragalus Polysaccharide Inhibits Autophagy and Apoptosis from Peroxide-Induced Injury in C2C12 Myoblasts, Cell Biochem Biophys 73(2) (2015) 433-9.

[46] Y. Lu, S. Li, H. Wu, Z. Bian, J. Xu, C. Gu, X. Chen, D. Yang, Beneficial effects of astragaloside IV against angiotensin II-induced mitochondrial dysfunction in rat vascular smooth muscle cells, Int J Mol Med 36(5) (2015) 1223-32.

[47] Y. Cao, T. Shen, X. Huang, Y. Lin, B. Chen, J. Pang, G. Li, Q. Wang, S. Zohrabian, C. Duan, Y. Ruan, Y. Man, S. Wang, J. Li, Astragalus polysaccharide restores autophagic flux and improves cardiomyocyte function in doxorubicin-induced cardiotoxicity, Oncotarget 8(3) (2017) 4837-4848.

[48] B.Y. Chiu, C.P. Chang, J.W. Lin, J.S. Yu, W.P. Liu, Y.C. Hsu, M.T. Lin, Beneficial effect of

astragalosides on stroke condition using PC12 cells under oxygen glucose deprivation and reperfusion, Cell Mol Neurobiol 34(6) (2014) 825-37.

[49] S. Lavandero, M. Chiong, B.A. Rothermel, J.A. Hill, Autophagy in cardiovascular biology, J Clin Invest 125(1) (2015) 55-64.

Figure Legends

Figure 1. Identification of photoaged rat dermal fibroblasts

A, SA-β-Gal staining of RDFs at 48h after treating with or without 6 exposures of UVB (4 mJ/cm^2). Quantitative analysis of SA-β-Gal-positive cells. At least 500 cells were counted in each well. B-C, Immunoblot and quantitative analysis of p21 and p53 expression level of RDFs under indicated doses of repeated UVB treatments. D, Detection of the mRNA level of p21, p16, IL-1β, IL-6, and TNFα of RDFs treated by 6 exposures of UVB (4 mJ/cm^2) using β-actin as loading control. Data are presented as means ± SD from three individual experiments; **P*<0.05, ***P*<0.01, ****P*<0.001.

Figure 2. AST suppress UVB-induced collagen-I degradation and photoaging

A, Immunoblot analysis of Col1 of RDFs treated by 0-5 mJ/cm^2 of UVB for 6 times. The relative protein expression of Col1 was quantified. B, Immunoblot analysis of Col1 of RFDs treated with or without 100 μg/ml of ASI, APS, ASF, and AST for 48h before 6 exposures of UVB (4 mJ/cm^2).CM refers to complete medium. The relative protein expression of Col1 was quantified. C, Immunoblot analysis of Col1 of RDFs treated by 6 exposures of UVB (4 mJ/cm^2) following with 0 to 100 μg/ml of AST for 48h. The relative protein expression of Col1 was quantified. D, SA-β-Gal staining of RDFs treated by 6 exposures of UVB (4 mJ/cm^2) with or without 100 μg/ml of AST for another 48h. Quantitative analysis of SA-β-Gal-positive cells. At least 500 cells were counted in each well. Data are presented as means ± SD from three individual experiments; **P*<0.05, ***P*<0.01, ****P*<0.001.

Figure 3. Anti-oxidative and cyto-protective effects of AST

A, Quantitative analysis of DCF-positive RDFs treated by 10 mJ/cm^2 of UVB after incubation with or without 100 μg/ml of AST for 24h. At least 600 random cells were scored for each group. B, RDFs were treated as (A), and stained by JC-1 after 24h of UVB irradiation. C, RDFs were treated by 0-10 mJ/cm^2 of UVB after incubation with or without 100 μg/ml of AST for 24h, cell viability of each group was measured by CCK-8 for another 24h. D, Immunoblot and quantitative analysis of cleaved caspase 3 and p53. Data are presented as means ± SD from three individual

experiments; *P<0.05, **P<0.01, ***P<0.001, NS: not significant.

Figure 4. AST repressed UVB-induced collagen-I reduction through ERK and p38 inhibition

A-B, Detection of the mRNA level of p21, IL-1β, IL-6, TNFα, MMP1, MMP3, MMP9, MMP13 and ICAM1 of RDFs treated with 6 exposures of UVB (4 mJ/cm^2) using β-actin as loading control. C, Immunoblot and quantitative analysis of Col1, P-p38, p38, phosphorylated ERK (p-ERK), and total ERK of RDFs treated by 6 exposures of UVB (4 mJ/cm^2) after incubation with or without 100 μg/ml of AST for 48h. Data are presented as means ± SD from three individual experiments; *P<0.05, **P<0.01, NS: not significant.

Figure 5. UVB-inhibited autophagy could be reversed by AST

A, Immunoblot and quantitative analysis of LC3 of RDFs treated by 6 exposures of UVB (4 mJ/cm^2) with or without 100 μg/ml of ASI, APS, ASF, and AST for another 48h. B, Immunoblot and quantitative analysis of LC3 and p62 of RDFs treated by 6 exposures of UVB (4 mJ/cm^2) with 0 to 100 μg/ml of AST for another 48h. C, Immunoblot and quantitative analysis of p62 and LC3 of RDFs treated by 100 μg/ml of AST with or without 10 μM of CQ and by 10 μM of CQ alone for 48h. D, Immunoblot analysis of p62 and LC3 of RDFs without exposures of UVB (4 mJ/cm^2) followed by 100 μg/ml of AST or 0.5 μM of rapamycin (Rap) plus 5 mM of 3-MA or 10 μM of CQ for 48h. Data are presented as means ± SD from three individual experiments; *P<0.05, **P<0.01, ***P<0.001.

Figure 6. AST upregulated UVB-reduced collagen-I by autophagy activation

A, Immunoblot analysis of Col1 and LC3 of RDFs treated by 6 exposures of UVB (4 mJ/cm^2) followed by 0 to 100 μg/ml of AST for 48h. B, Immunoblot analysis of Col1 and p62 of RDFs treated by 6 exposures of UVB (4 mJ/cm^2) followed by 100 μg/ml of AST plus 5 mM of 3-MA for 48h. C, Immunoblot analysis of Col1 and p62 of RDFs treated by 6 exposures of UVB (4 mJ/cm^2) followed by 100 μg/ml of AST plus 10 μM of CQ for 48h. D, Immunoblot analysis of Col1 of normal RDFs without repeated UVB irradiation treated by 100 μg/ml of AST or 0.5 μM of rapamycin (Rap) with or without 5 mM of 3-MA or 10 μM of CQ for 48h. Data are presented as means ± SD from three individual experiments; *P<0.05, **P<0.01, ***P<0.001, NS: not

significant

Figure 7. Putative model of the signaling pathways of AST in protecting photoaged cells from UVB-induced senescence

Table 1. Primers for real time PCR

Target Gene	Sequence
p21	F: TGTGATATGTACCAGCCACAGG
	R: CGAACAGACGACGGCATACT
p16	F: CTCCGAGAGGAAGGCGAAC
	R: TTGCCCATCATCATCACCTGTA
IL-1β	F: GCTTCCTTGTGCAAGTGTCT
	R: TCTGGACAGCCCAAGTCAAG
IL-6	F: CATTCTGTCTCGAGCCCACC
	R: GCTGGAAGTCTCTTGCGGAG
TNFα	F: GATCGGTCCCAACAAGGAGG
	R: CTTGGTGGTTTGCTACGACG
MMP1	F: TCAGCATGCTTAGCCTTCCT
	R: AGGTATTTCCAGACTGTTTCCAC
MMP3	F: TTTGGCCGTCTCTTCCATCC
	R: GCATCGATCTTCTGGACGGT
MMP9	F: GCTGGCAGAGGATTACCTGT
	R: TGGCCTTTAGTGTCTCGCTG
MMP13	F: GACAAGCAGCTCCAAAGGCTA
	R: AGCTCATGGGCAGCAACAAT
ICAM	F: ACAGCTCCTCTCGGGAAATG
	R: CAACAGTAAATGGTTTCTCTTGAAC
β-actin	F: AGATCAAGATCATTGCTCCTCCT
	R: ACGCAGCTCAGTAACAGTCC

Figure S1. Identification of rat dermal fibroblasts and the influence of UVB on JNK pathway

A, Immunostaining of isolated RDFs by vimentin antibody (green), and nuclei staining by hoeschst33342 (blue). B, Immunoblot analysis of phosphorylated p38 (p-p38), total p38 of RDFs treated by 0-5 mJ/cm^2 of UVB for total 6 times. C, Immunoblot analysis of phosphorylated JNK (p-JNK), total JNK of RDFs treated by 0, 2, 3, 4, 5 mJ/cm^2 of UVB for total 6 times in 3 days.

Figure S2. Repeated UVB irradiation inhibited the expression of collagen-I and autophagy by a dose-dependent manner

A, Immunoblot and quantitative analysis of LC3 of RDFs treated by 0-5 mJ/cm^2 of UVB for 6 times. Data are presented as means ± SD from three individual experiments. B, Immunoblot analysis of Col1 and LC3 of RDFs by 0-5 mJ/cm^2 of UVB for 6 times; *P<0.05.

Fig. 1

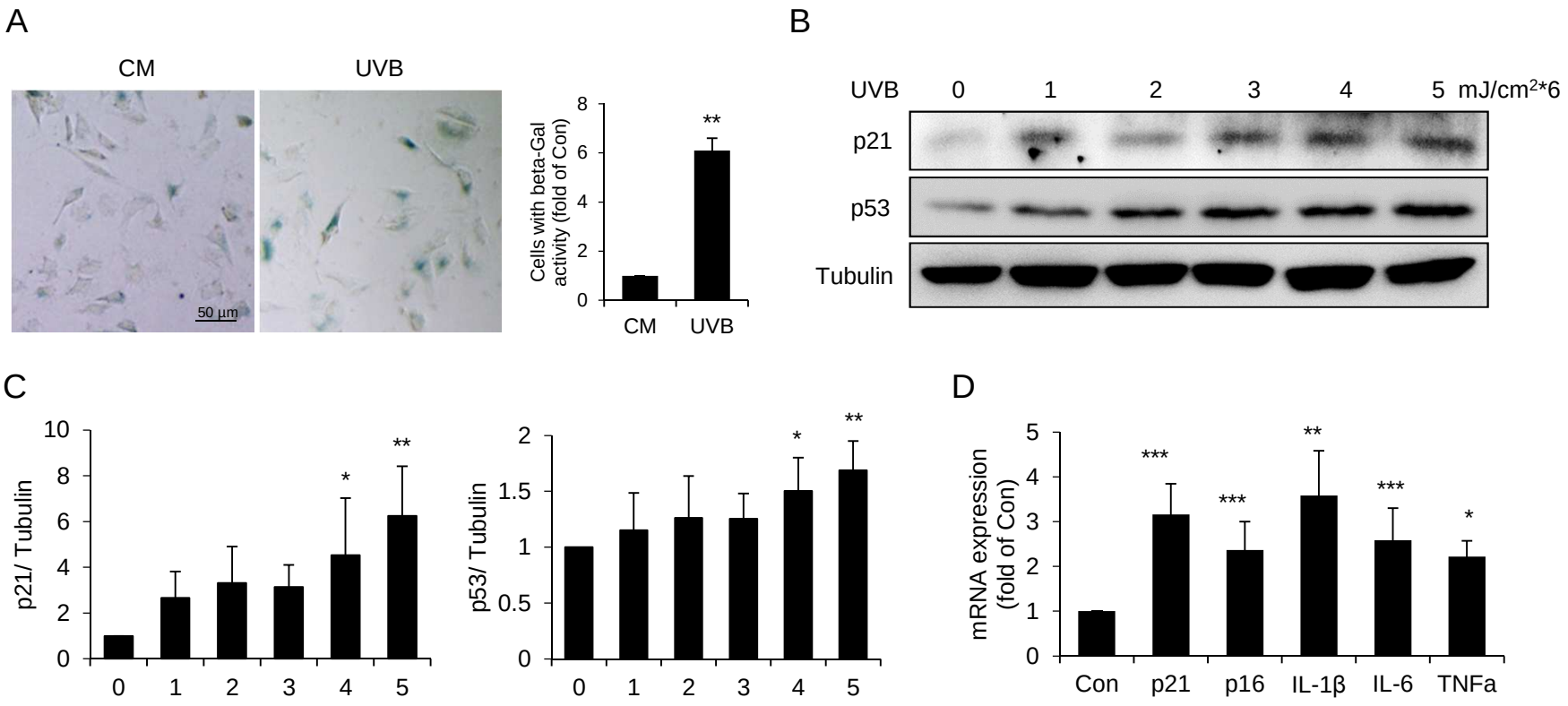
A
CM
UVB
50 μm
Cells with beta-Gal activity (fold of Con)
**
CM
UVB
B
UVB 0 1 2 3 4 5 mJ/cm²*6
p21
p53
Tubulin
C
p21/ Tubulin
*
**
p53/ Tubulin
*
**
0 1 2 3 4 5
D
mRNA expression (fold of Con)
***
***
**
***
*
Con
p21
p16
IL-1β
IL-6
TNFa

Fig. 2

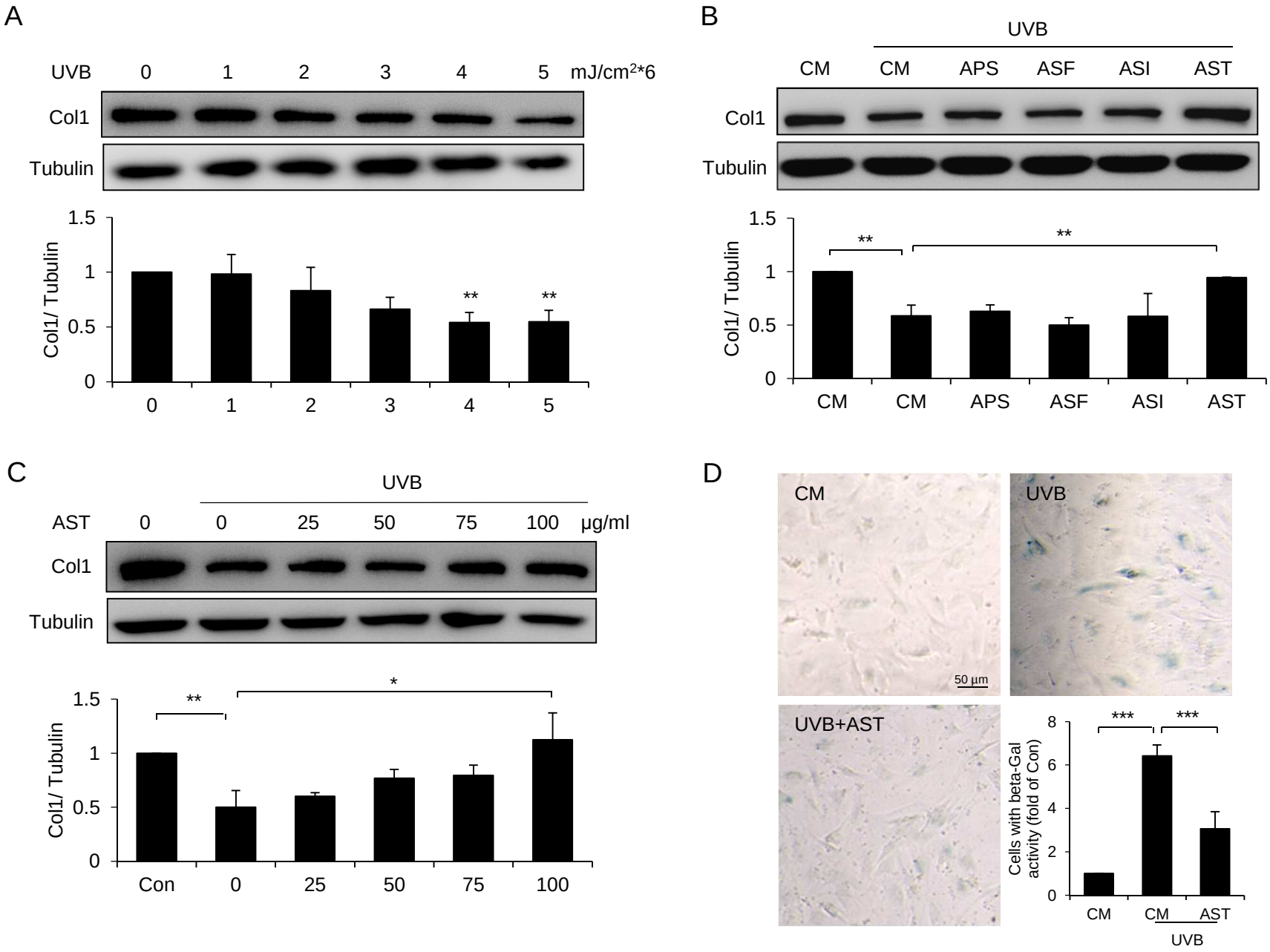
A
UVB 0 1 2 3 4 5 mJ/cm2*6
Col1
Tubulin
Col1/ Tubulin
1.5
1
0.5
0
**
**
0 1 2 3 4 5
B
UVB
CM CM APS ASF ASI AST
Col1
Tubulin
Col1/ Tubulin
1.5
1
0.5
0
**
**
CM CM APS ASF ASI AST
C
UVB
AST 0 0 25 50 75 100 μg/ml
Col1
Tubulin
Col1/ Tubulin
1.5
1
0.5
0
**
*
Con 0 25 50 75 100
D
CM
UVB
UVB+AST
50 μm
Cells with beta-Gal activity (fold of Con)
8
6
4
2
0
***
***
CM CM AST
UVB

Fig. 3

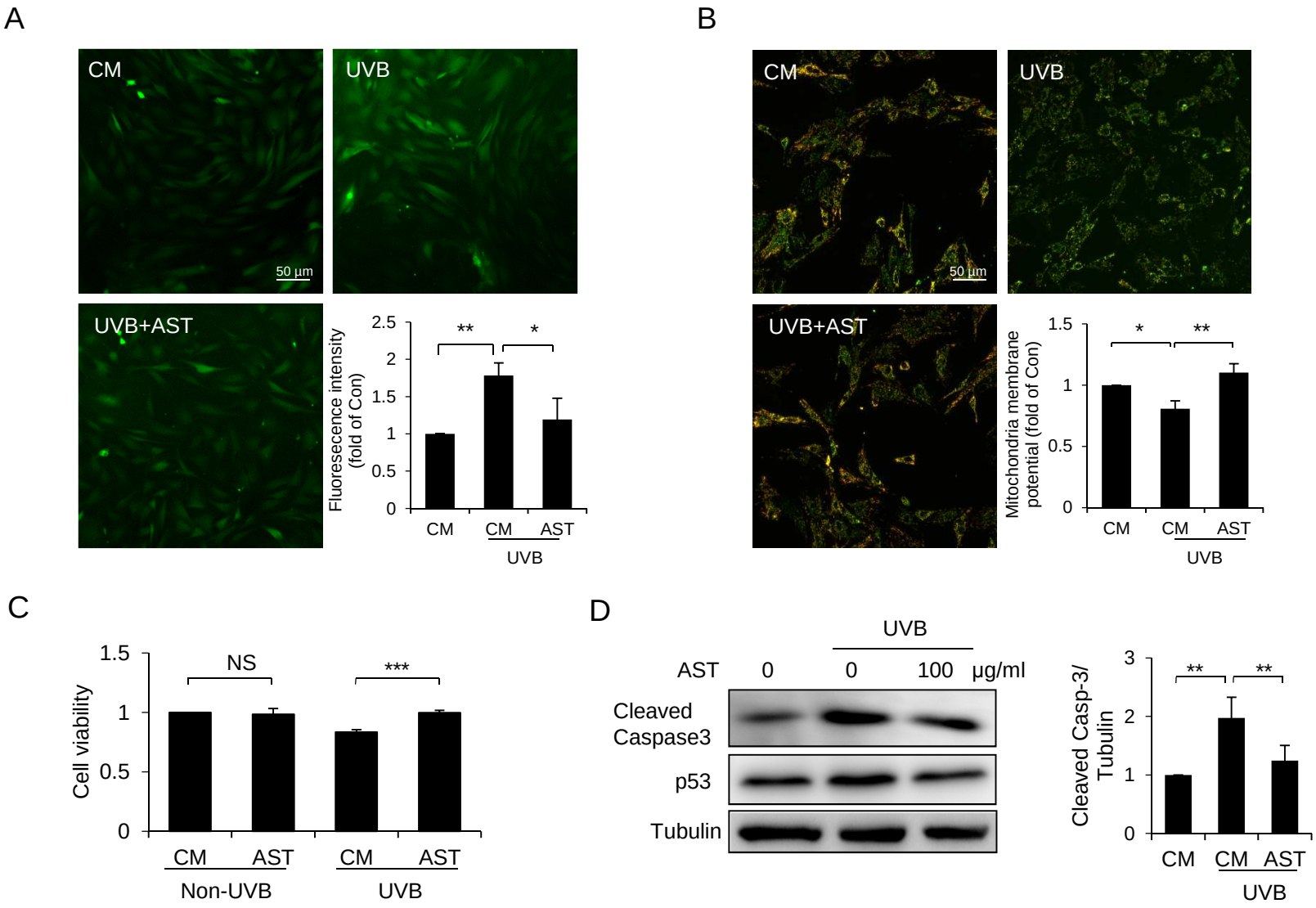
A
CM
UVB
50 μm
UVB+AST
Fluorescence intensity (fold of Con)
2.5
2
1.5
1
0.5
0
**
*
CM
CM
AST
UVB
B
CM
UVB
50 μm
UVB+AST
Mitochondria membrane potential (fold of Con)
1.5
1
0.5
0
*
**
CM
CM
AST
UVB
C
Cell viability
1.5
1
0.5
0
NS
***
CM
AST
CM
AST
Non-UVB
UVB
D
UVB
AST
0
0
100
μg/ml
Cleaved Caspase3
p53
Tubulin
Cleaved Casp-3/ Tubulin
3
2
1
0
**
**
CM
CM
AST
UVB

Fig. 4

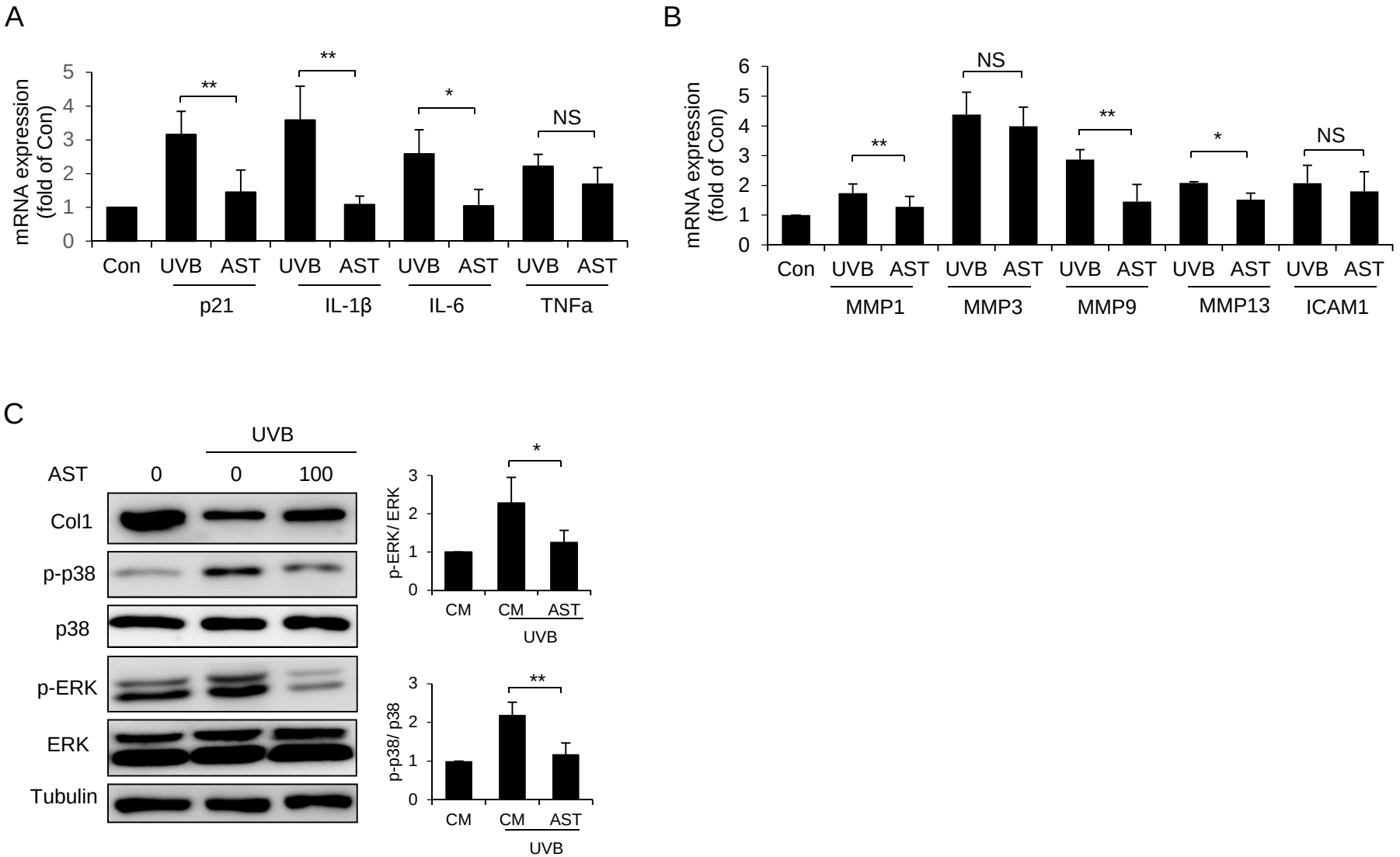
A
mRNA expression (fold of Con)
Con
UVB
AST
p21
IL-1β
IL-6
TNFa
**
*
NS
B
MMP1
MMP3
MMP9
MMP13
ICAM1
C
UVB
AST
0
100
Col1
p-p38
p38
p-ERK
ERK
Tubulin
p-ERK/ ERK
p-p38/ p38
CM

Fig. 5

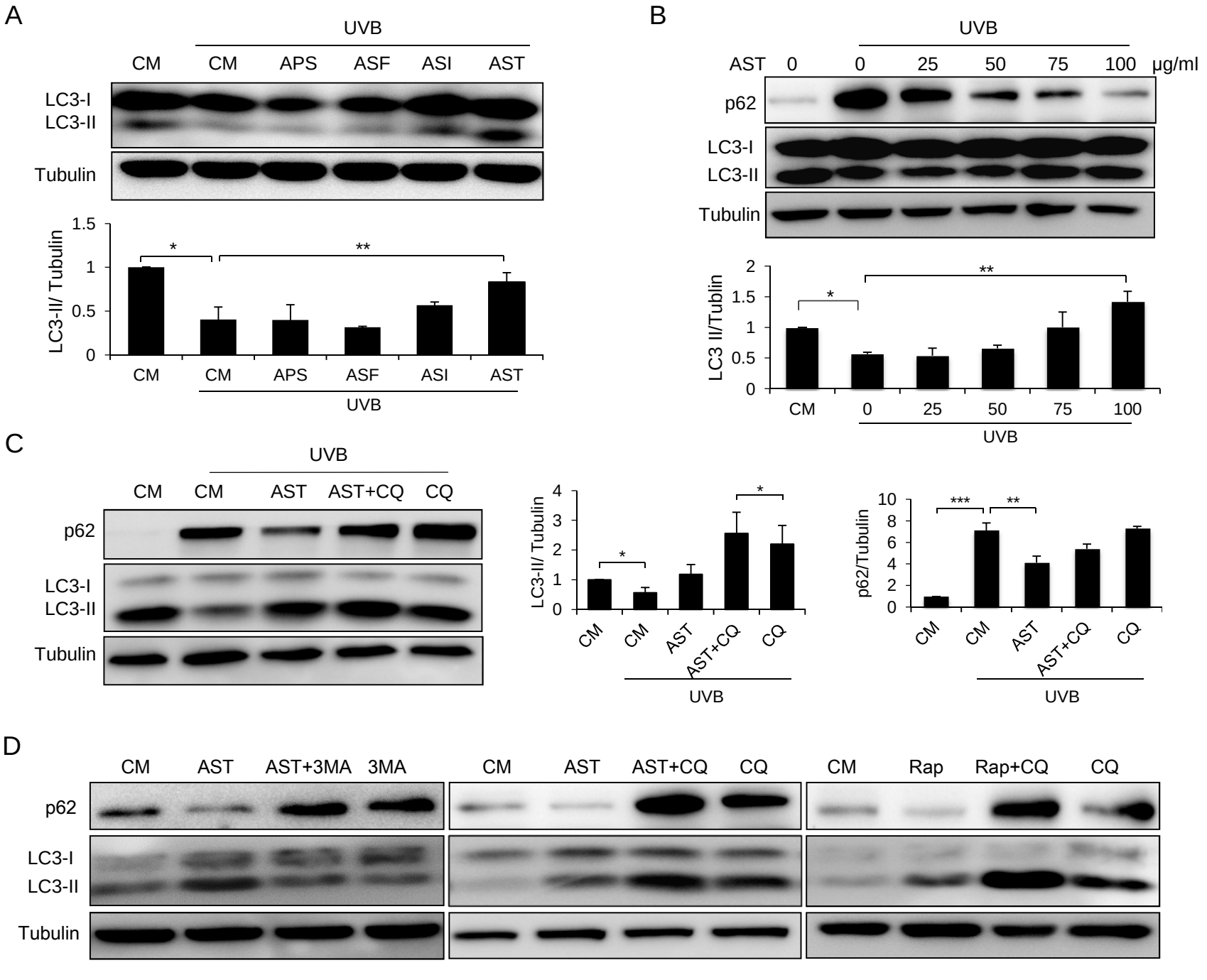
A
UVB
CM
CM
APS
ASF
ASI
AST
LC3-I
LC3-II
Tubulin
LC3-II/ Tubulin
1.5
1
0.5
0
*
**
CM
CM
APS
ASF
ASI
AST
UVB
B
UVB
AST
0
0
25
50
75
100
μg/ml
p62
LC3-I
LC3-II
Tubulin
LC3 II/Tublin
2
1.5
1
0.5
0
*
**
CM
0
25
50
75
100
UVB
C
UVB
CM
CM
AST
AST+CQ
CQ
p62
LC3-I
LC3-II
Tubulin
LC3-II/ Tubulin
4
3
2
1
0
*
*
CM
CM
AST
AST+CQ
CQ
UVB
p62/Tubulin
10
8
6
4
2
0
***
**
CM
CM
AST
AST+CQ
CQ
UVB
D
CM
AST
AST+3MA
3MA
CM
AST
AST+CQ
CQ
CM
Rap
Rap+CQ
CQ
p62
LC3-I
LC3-II
Tubulin

Fig. 6

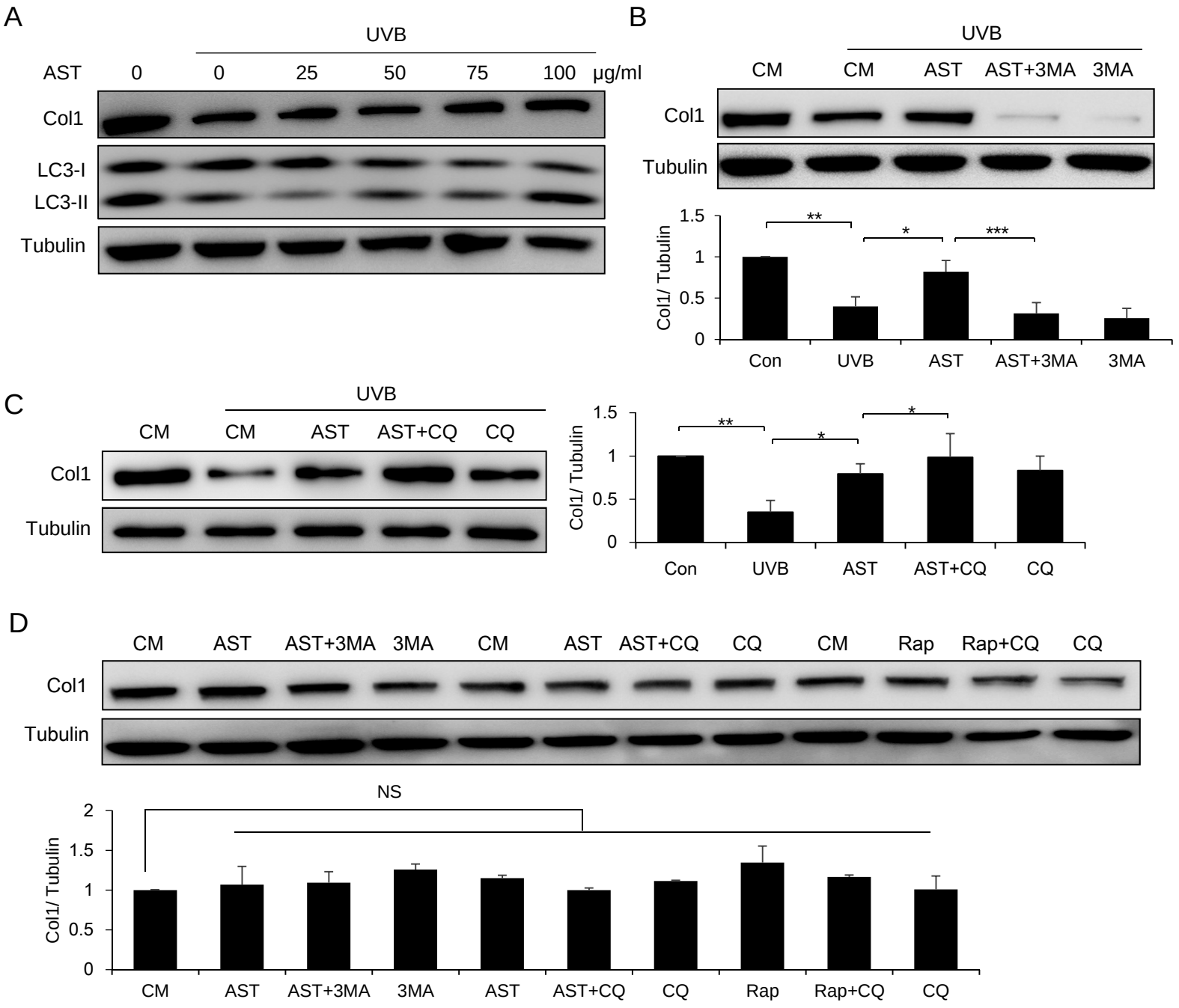
A
UVB
AST 0 0 25 50 75 100 μg/ml
Col1
LC3-I
LC3-II
Tubulin
B
UVB
CM CM AST AST+3MA 3MA
Col1
Tubulin
Col1/ Tubulin
1.5
1
0.5
0
**
*
***
Con UVB AST AST+3MA 3MA
C
UVB
CM CM AST AST+CQ CQ
Col1
Tubulin
Col1/ Tubulin
1.5
1
0.5
0
**
*
*
Con UVB AST AST+CQ CQ
D
CM AST AST+3MA 3MA CM AST AST+CQ CQ CM Rap Rap+CQ CQ
Col1
Tubulin
NS
Col1/ Tubulin
2
1.5
1
0.5
0
CM AST AST+3MA 3MA AST AST+CQ CQ Rap Rap+CQ CQ

Fig. 7

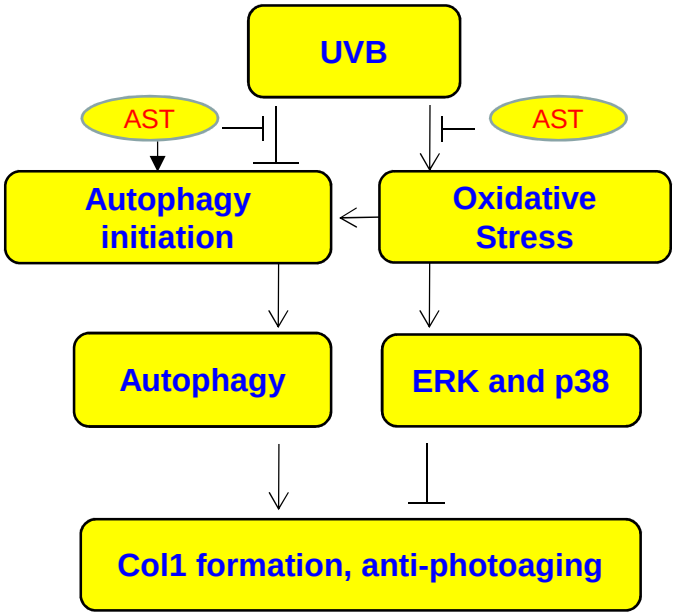

Fig. S1

A

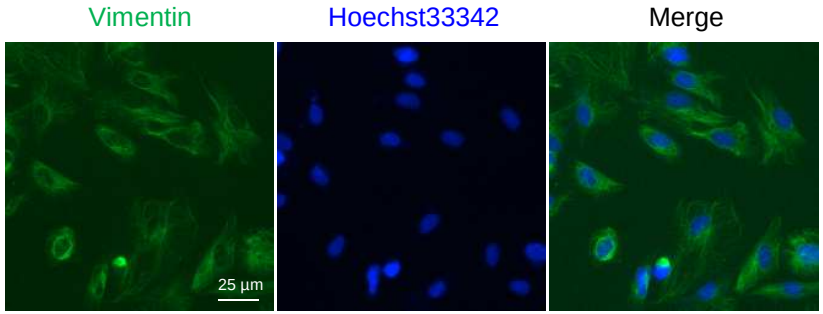

B

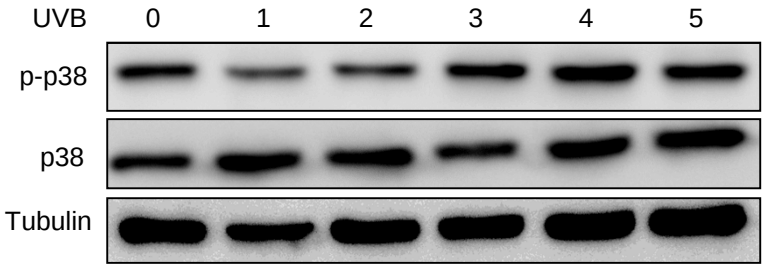

C

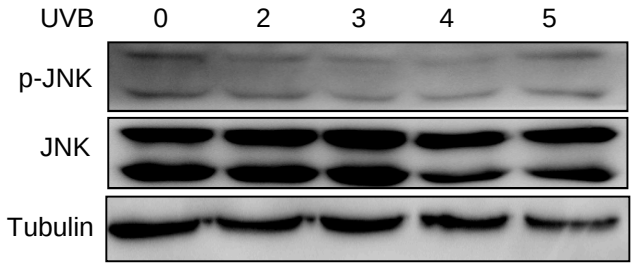

Fig. S2